Persistence to High Temperatures of Interlayer Coherence in an Organic Superconductor

John Singleton,[1] P. A. Goddard,[1,2] A. Ardavan,[2] A. I. Coldea,[3] S. J. Blundell,[2]
R. D. McDonald,[1] S. Tozer,[4] and J. A. Schlueter[5]

[1]*National High Magnetic Field Laboratory, Los Alamos National Laboratory, Los Alamos, New Mexico 87545, USA*
[2]*Department of Physics, University of Oxford, The Clarendon Laboratory, Parks Road, Oxford OX1 3PU, United Kingdom*
[3]*H.H. Wills Physics Laboratory, Bristol University, Tyndall Avenue, Bristol, BS9 1TL, United Kingdom*
[4]*NHMFL, 1800 E. Paul Dirac Drive, Tallahassee Florida 32310, USA*
[5]*Materials Science Division, Argonne National Laboratory, Argonne, Illinois 60439, USA*

(Received 11 October 2006; published 13 July 2007)

The interlayer magnetoresistance ρ_{zz} of the organic metal κ-(BEDT-TTF)$_2$Cu(NCS)$_2$ is studied in fields of up to 45 T and at temperatures T from 0.5 to 30 K. The peak in ρ_{zz} seen in in-plane fields, a definitive signature of interlayer coherence, remains to Ts exceeding the Anderson criterion for incoherent transport by a factor $\sim$30. Angle-dependent magnetoresistance oscillations are modeled using an approach based on field-induced quasiparticle paths on a 3D Fermi surface, to yield the T dependence of the scattering rate τ^{-1}. The results suggest that τ^{-1} does not vary strongly over the Fermi surface, and that it has a T^2 dependence due to electron-electron scattering.

DOI: 10.1103/PhysRevLett.99.027004 PACS numbers: 74.70.Kn, 71.20.Rv, 78.20.Ls

The past two decades have seen a blossoming of interest in compounds with quasi-two-dimensional (Q2D) electronic band structures; examples include layered oxides [1–3] and crystalline organic metals [4–13]. These materials may be described by a tight-binding Hamiltonian in which the ratio of the interlayer transfer integral $t_\perp$ to the average intralayer transfer integral $t_{||}$ is $\ll 1$ [4–7,11,14]. The question arises as to whether the interlayer charge transfer is coherent or incoherent in these materials, i.e., whether or not the Fermi surface (FS) is three dimensional (3D), extending in the interlayer direction [2,6,7,11,14]. Various criteria for interlayer incoherence have been proposed, including (Ref. [2], p. 50)

$$k_B T > t_\perp, \tag{1}$$

where T is the temperature. In this picture, thermal fluctuations "wipe out" the interlayer dispersion [2].

Interlayer incoherence is thought to be important in Q2D materials ranging from graphite to selenides [15]: it may be pivotal in the mechanism for cuprate superconductivity [2]; it may lead to non-Fermi-liquid behavior [3,14]; and it may determine an organic metal's predisposition to superconductivity or density-wave formation [16]. Proposals that the stripe phases of many oxides are due to FS instabilities (in materials often classed as insulators) [17], strongly suggest that criteria used to denote coherent band transport should be reviewed [15]. In view of this activity, it is vital to test assertions such as Eq. (1). To this end, we have measured the field-orientation-dependent magnetoresistance (MR) of the organic metal κ-(BEDT-TTF)$_2$Cu(NCS)$_2$ using fields of up to 45 T and Ts of up to 30 K (Fig. 1). This material was chosen because its FS is well known [16,18] [Fig. 2(c)]; previous low-T experiments have shown that the interlayer transfer integral is $t_{\mathbf{a}} = 0.065 \pm 0.007$ meV [18–20] and modest Ts allow the inequality in Eq. (1) to be greatly exceeded ($t_{\mathbf{a}}/k_B \approx$ 0.5 K). Previous studies show that MR is a useful probe of FS dimensionality [4–11,18] and the effects of disorder on interlayer coherence [7]. Here, such techniques demonstrate that interlayer coherence survives to at least $k_B T \gtrsim \sim 30 t_{\mathbf{a}}$ [cf. Eq. (1)]. In addition, our data determine the low-T quasiparticle scattering rate τ^{-1}. Recent works stress that the effects of scattering in organic metals can give information about the mechanism for superconductivity [21,22].

Electrical contacts (resistance $\sim 10\ \Omega$) are made to single crystals ($\sim 0.7 \times 0.5 \times 0.1$ mm^3) of κ-(BEDT-TTF)$_2$Cu(NCS)$_2$ using 12.5 μm Pt wire bonded by graphite paste. Current and voltage terminals are arranged such that the measured resistance R_{zz} is proportional to the interlayer component of the MR tensor, ρ_{zz} [18,19]. The data in Figs. 1 and 2 are for a well-characterized crystal also employed in Refs. [11,18,23]. Additional experiments (e.g., Fig. 3) use $d8$-κ-(BEDT-TTF)$_2$Cu(NCS)$_2$ crystals; here, "$d8$" indicates that the hydrogens of BEDT-TTF are replaced by deuterium. These crystals were studied in Ref. [18]; it was found that deuteration reduces $t_{\mathbf{a}}$ to 0.045 ± 0.005 meV. Samples are mounted on a ceramic holder attached to a cryogenic goniometer allowing continuous rotation in static magnetic fields $\mathbf{B}$. Crystal orientations are labeled by the angles θ, ϕ shown in Fig. 1 (inset). Sample Ts are stabilized using a calibrated Cernox sensor on the sample holder and a heater driven by a feedback circuit. The Cernox is monitored during isothermal $\mathbf{B}$ sweeps to deduce corrections to the apparent T due to MR; results are in good agreement with Ref. [24]. Static fields are provided by the 45 T Hybrid magnet at NHMFL Tallahassee and 33 T Bitter magnets at NHMFL and HFML Nijmegen.

Typical R_{zz} data are shown in Figs. 1(a) ($\phi = 160°$) and 1(b) ($\phi = 90°$) for Ts in the range 5.3 to 29.3 K. For $\phi = 160°$, features in ρ_{zz} are known to be due to orbits on the

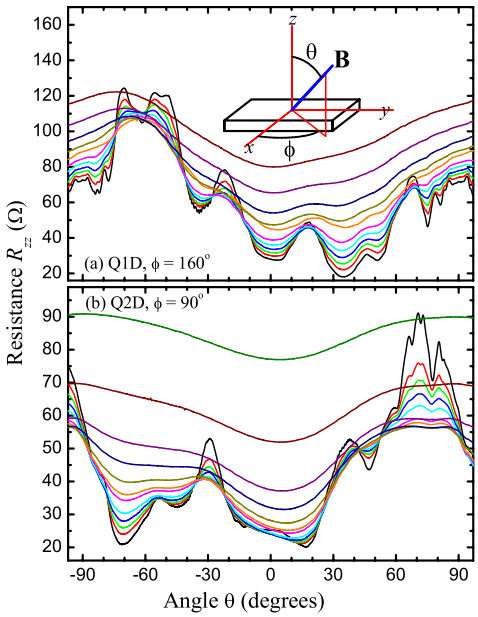

FIG. 1 (color online). Interlayer resistance $R_{zz}(\propto \rho_{zz})$ of a κ-(BEDT-TTF)$_2$Cu(NCS)$_2$ crystal versus tilt angle θ (see inset) for various constant T; $B = 45$ T. (a) Data for $\phi = 160°$, a rotation plane at which ρ_{zz} is determined by phenomena on the Q1D FS sections. In order of increasing R_{zz} at $\theta = 35°$, the curves are for $T = 5.3$, 6.5, 7.6, 8.6, 9.6, 10.6, 12.1, 13.1, 14.6, 17.1, 19.6, and 29.3 K, respectively. In addition to AMROs, DKCOs can be seen as twin peaks on either side of $\theta = 90°$ in the lower-T data. (b) Similar data for $\phi = 90°$; here ρ_{zz} features are associated with the Q2D FS section. In order of increasing R_{zz} at $\theta = -70°$, the curves are for $T = 5.3$, 7.6, 8.6, 9.6, 10.6, 12.1, 13.1, 14.6, 17.1, 19.6, 24.5, and 29.3 K, respectively. The inset shows coordinates describing the sample's rotation about an axis in its Q2D planes. Angle θ is between **B** and z, the normal to the Q2D planes; ϕ is the angle between the plane of rotation and x, the $k_{\mathbf{b}}$ direction [18].

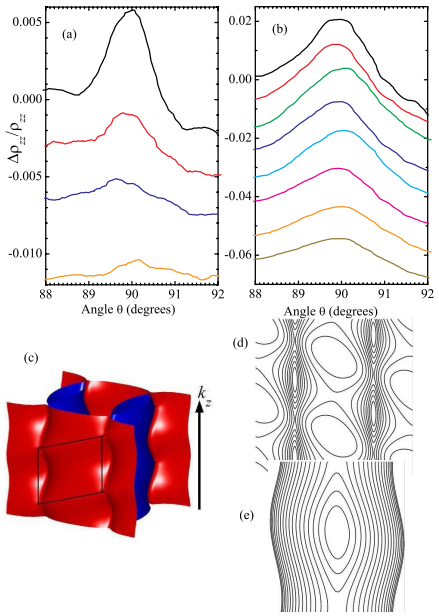

FIG. 2 (color online). (a) The 45 T magnetoresistance close to $\theta = 90°$ at $\phi = 160°$, plotted as $\Delta\rho_{zz}/\rho_{zz\mathrm{BG}}$, the fractional change in ρ_{zz} from the more slowly varying background. Data for $T = 5.3$ (highest), 7.6, 9.6, and 13.1 K (lowest) are shown, offset for visibility. (b) Similar data for $\phi = 90°$; the traces are for $T = 5.3$ (highest), 7.6, 8.6, 9.6, 10.6, 12.1, 13.1, and 14.6 K (lowest). Each trace has been offset for clarity. (c) 3D representation of the FS of κ-(BEDT-TTF)$_2$Cu(NCS)$_2$ (after Ref. [18]); the finite $t_{\mathbf{a}}$ gives the corrugations (greatly exaggerated) on the sides of the FS. Q1D and Q2D FS sections are shown in red and blue, respectively. (d) Consequent field-induced closed orbits on the side of the Q1D FS section when $\theta = 90°$ and $\phi = 0$. (e) Similar closed orbits on the Q2D FS section when $\theta = 90°$ and $\phi = 90°$. Orbits such as those in (d) and (e) give rise to the SQUIT peak in ρ_{zz}.

Q1D FS sections [18], whereas for $\phi = 90°$ they can be confidently attributed to Q2D FS orbits [18]. A series of angle-dependent MR oscillations (AMROs), periodic in $\tan\theta$ [16,18] is observed at both ϕ; those due to the Q2D FS sections are often known as *Yamaji oscillations* [16,25]. In addition, *Danner-Kang-Chaikin oscillations* (DKCOs) [18,26] are observed as peaks either side of $\theta = \pm 90°$ when $\phi = 160°$. As T increases, the AMROs decrease in intensity, with the higher-index oscillations (i.e., those closer to $\theta = 90°$ [18]) disappearing first. After most AMROs disappear, the slowly-varying background MR begins to increase more markedly.

Figures 2(a) and 2(b) show expansions of data in Fig. 1 close to $\theta = 90°$ at selected Ts. For ease of comparison, data are plotted as $\Delta\rho_{zz}/\rho_{zz\mathrm{BG}}$, the fractional deviation in ρ_{zz} from the background MR $\rho_{zz\mathrm{BG}}$ determined by fitting a smoothly varying curve through data either side of $\theta = 90°$ [11]. In such measurements, interlayer coherence is detected using the "coherence peak" or "Suppression of QUasiparticle Interlayer Transport" (SQUIT) peak [4–11,18], a maximum in $\Delta\rho_{zz}/\rho_{zz\mathrm{BG}}$ observed when **B** lies exactly in the intralayer plane (i.e., at $\theta = 90°$). This occurs because of the efficient interlayer velocity averaging caused by closed orbits on the side of the FS [Figs. 2(c)–2(e)]; these exist if, *and only if* [4–11,18], the interlayer transport is coherent; i.e., the FS is 3D. In Figs. 2(a) and 2(b), the SQUIT peak is visible close to $\theta = 90°$; in spite of the small $t_{\mathbf{a}}$, this demonstration of interlayer coherence persists to at least 14.6 K, exceeding the criterion in Eq. (1) by a factor of $\sim$30 [27].

The AMROs and DKCOs in Fig. 1 are similar to those observed at $T = 0.5$ K [18], the only difference being that they decrease in amplitude as T increases; i.e., the MR features do not change in form or angular position as T grows, but merely fade gradually. This suggests that the same mechanism is responsible for the form of the MR at all T examined. Moreover, the SQUIT peak (Fig. 2) demonstrates that the FS of κ-(BEDT-TTF)$_2$Cu(NCS)$_2$ is 3D up to at least $T \approx 15$ K [27]. We therefore simulate the

data using the numerical method based on field-induced quasiparticle trajectories across a 3D FS that was used to model $T = 0.5$ K AMRO results in Ref. [18]. This employs the Chambers' equation and the experimentally deduced FS [Fig. 2(c) [18]]; given $\mathbf{B}$ and θ, ϕ, the only input parameter required to calculate ρ_{zz} is τ. The model has the restriction that magnetic breakdown between the Q1D and Q2D FS sections [29] is not included; it is known that breakdown in κ-(BEDT-TTF)$_2$Cu(NCS)$_2$ can produce a series of AMROs [30]. However, the breakdown amplitude falls off rapidly with increasing θ [29], so that these effects are small for $B \approx 45$ T when $\theta \gtrsim 70°$ [30]. In the following, we neglect lower θ data for this reason.

Typical comparisons of experiment and simulation are in Figs. 3(a) and 3(b) ($\phi = 15°$). For each ϕ, one can map the normalized AMRO amplitude $\Delta R_{zz}/\langle R_{zz}\rangle$ [see Fig. 3(c)] from the simulation onto the experimental value by adjusting τ. Moreover, for each T, the same τ, to within experimental errors, fits all the AMRO features. This suggests that *all* AMRO amplitudes for a particular ϕ are described by the parameter $\omega\tau$, where ω is the angular frequency for the orbit responsible for the AMRO feature. In the case of AMROs due to the Q2D FS sections, $\omega = (eB/m^*_\alpha)\cos\theta$, the cyclotron frequency [18]. Here, m^*_α is the $\theta = 0$ effective mass of the α Q2D pocket of the FS [16,29]. For Q1D AMROs, the relevant period is the time for a quasiparticle to cross the Brillouin zone on the Q1D FS sheet [31]. As long as one avoids the region close to $\theta = 90°$ where the SQUIT and DKCOs occur (the latter involving orbits that "snake" across contours on the FS [18,26]), this frequency can be expressed as $\omega = [2eB/(m^*_\beta - m^*_\alpha)]\cos\theta$, where m^*_β is the $\theta = 0$ effective mass of the "β" breakdown orbit [29].

Using these ωs, the $\Delta R_{zz}/\langle R_{zz}\rangle$ values of *all* of the AMRO features at a particular ϕ collapse onto a single curve as a function of $\omega\tau$; an example is shown in Fig. 3(d) for AMROs due to the Q2D FS. Once this is known for each ϕ, τ can be readily found from AMRO data. The τ values deduced follow a T dependence of the form $\tau^{-1} = \tau_0^{-1} + AT^2$ closely. Moreover, to within experimental errors, the same values of τ_0 and A are obtained, irrespective of the FS orbits involved. Two examples are in Fig. 4, which shows τ deduced from AMROs at $\phi = 160°$ [(a)- due to Q1D FS sections] and $\phi = 90°$ [(b)- due to Q2D FS sections]. In spite of the fact that the quasiparticle orbits involved are very different, and involve distinct FS sections, the T dependence of τ is virtually identical. This suggests that mechanisms for superconductivity in organic metals that invoke a large variation in τ^{-1} over the FS (e.g., "FLEX"methods [32]) are inappropriate for

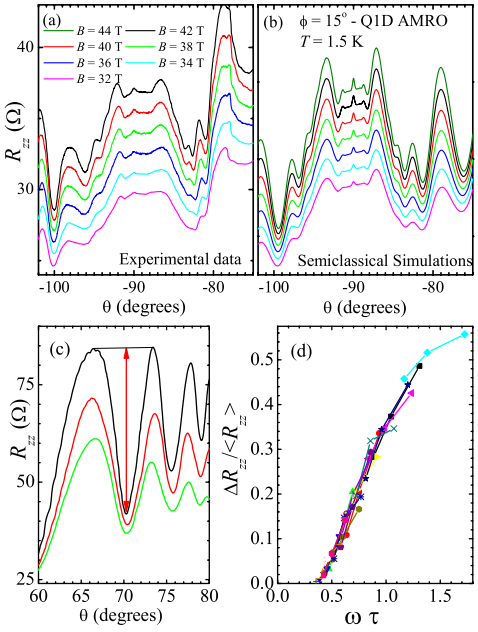

FIG. 3 (color online). Comparison of experimental ρ_{zz} data (a) and the numerical simulations (b). $T = 1.5$ K and $\phi = 15°$; for the lowest to the highest traces, B is 32, 34, 36, 38, 40, 42, and 44 T (no offset is applied). (c) AMRO data for $\phi = 150°$, $T = 1.5$ K and fields of 20 (lowest), 24, and 28 T (highest). The arrow indicates the amplitude ΔR_{zz} of a particular AMRO feature; $\langle R_{zz}\rangle$ is the resistance at the arrow's midpoint. (d) Experimental AMRO $\Delta R_{zz}/\langle R_{zz}\rangle$ for $\phi = 150°$ plotted versus orbit angular frequency ω times scattering time τ. Data for several AMROs, denoted by their Yamaji indices [16] i are shown [$i = 2$ (square), $i = 3$ (dot), $i = 4$ (triangle) and $i = 5$ (inverted triangle)] for several Ts in the range 1.7 to 5.5 K.

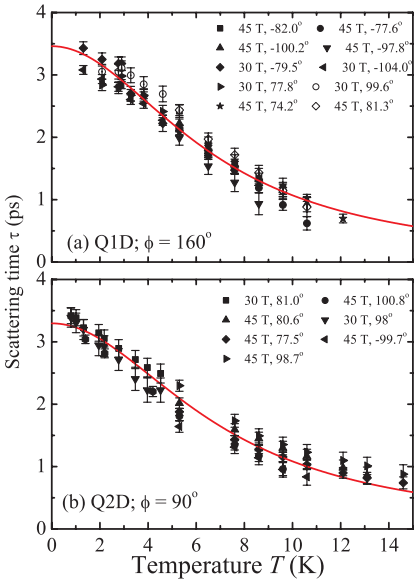

FIG. 4 (color online). Scattering time τ deduced from AMROs at $\phi \approx 160°$ (a) and $\phi \approx 90°$ (b) versus T. Consistent values of τ are deduced from several AMRO features at fields of 30 and 45 T (insets show field and θ for each feature). The data are fitted to $\tau = (\tau_0^{-1} + AT^2)^{-1}$ (curves) with $\tau_0 = 3.3 \pm 0.1$ ps and $A = 0.0062 \pm 0.0003$ ps^{-1} K^{-2} (a) and $\tau_0 = 3.5 \pm 0.1$ ps and $A = 0.0065 \pm 0.0003$ ps^{-1} K^{-2} (b). These $\tau(T)$ values are identical to within experimental errors.

κ-(BEDT-TTF)$_2$Cu(NCS)$_2$. For all FS orbits studied, $\tau_0 = 3.4 \pm 0.2$ ps (Fig. 4); this is, as expected [33], somewhat longer than the "Dingle" scattering time deduced from the B dependence of the Shubnikov–de Haas oscillations (2.3 ± 0.2 ps) [18] and similar to those observed in GHz magnetoconductivity [23].

The T^2 dependence of τ^{-1} suggests electron-electron scattering [34]. A T^2 scattering rate was inferred from $B = 0$ resistivity measurements [35]. However, problems in deconvolving the in-plane resistivity $\rho_{||}$ from ρ_{zz} in experimental data [16,23], and the influence of the broad superconducting transition on the T dependence of the measured resistivity [16] mean that this attribution cannot be considered conclusive. By contrast, the T-dependent AMROs provide an unambiguous gauge of the scattering rate of normal-state quasiparticles, allowing the mechanism to be definitively identified.

When $k_BT > 4t_{\mathbf{a}}$, the interlayer contribution to the bandwidth [20], the FS shown in Fig. 2(c) is "blurred" on a wave vector scale $k_BT/\hbar v_F$ (where v_F is the Fermi velocity) exceeding the amplitude of interlayer corrugation. Nevertheless, a Fermi-liquid picture predicts that the semiclassical dynamics of each quasiparticle are still governed by an equation of motion which reflects the detailed nature of the interlayer dispersion. Quasiparticle states within $\sim k_BT$ of the chemical potential continue to contribute to the AMROs and SQUIT, as long as the underlying dispersion is not affected by a variation in electron energy on the scale of k_BT; this will hold when $k_BT \ll t_{||} \sim 10 - 100$ meV [18]. Then, the only effect of raising T is from T-dependent contributions to the scattering rate. This is exactly what we find in our AMRO data, and demonstrates that a coherent 3D FS picture is valid for this compound, at least at $k_BT \lesssim 0.1t_{||}$ [36].

In summary, the angle-dependent interlayer magnetoresistance ρ_{zz} of κ-(BEDT-TTF)$_2$Cu(NCS)$_2$ has been studied in fields of up to 45 T as a function of temperature T. The SQUIT in ρ_{zz} seen in exactly in-plane fields, a definitive signature of a 3D Fermi surface, persists to Ts exceeding the Anderson proposal for incoherent transport [Eq. (1) [2]] by a factor $\sim$30. Features in ρ_{zz} have been successfully modeled using an approach based on field-induced quasiparticle paths on a 3D Fermi surface, to yield the T dependence of the quasiparticle scattering rate τ^{-1}. The results suggest that τ^{-1} does not vary strongly over the Fermi surface, and that it follows a T^2 dependence due to electron-electron scattering.

This work is funded by U. S. Department of Energy (DOE) Grant No. LDRD 20030084DR and by EPSRC (UK). NHMFL is supported by NSF, DOE, and the State of Florida, and HFMLNijmegen by EuroMagNET, EU Contract No. RII3-CT-2004-506239. Work at Argonne was supported by the Office of Basic Energy Sciences, DOE, Contract No. W-31-109-ENG-38. P. A. G. and A. A. acknowledge support from the Glasstone Foundation and the Royal Society, respectively. N. Harrison, R. McKenzie, and N. Shannon are thanked for helpful discussions.

[1] N. E. Hussey, J. Phys. Chem. Solids **67**, 227 (2006).
[2] P. W. Anderson, *The Theory of Superconductivity in the High T_c Cuprates* (Princeton University, Princeton, N J, 1997).
[3] N. Shannon *et al.*, Phys. Rev. B **55**, 12963 (1997).
[4] R. H. McKenzie and P. Moses, Phys. Rev. Lett. **81**, 4492 (1998).
[5] N. Hanasaki *et al.*, Phys. Rev. B **57**, 1336 (1998).
[6] J. Wosnitza *et al.*, Phys. Rev. B **65**, 180506(R) (2002).
[7] M. V. Kartsovnik *et al.*, Phys. Rev. Lett. **96**, 166601 (2006).
[8] S. Uji *et al.*, Phys. Rev. B **68**, 064420 (2003).
[9] K. Enomoto *et al.*, Phys. Rev. B **73**, 045115 (2006).
[10] M. Kuraguchi *et al.*, Synth. Met. **133–134**, 113 (2003).
[11] J. Singleton *et al.*, Phys. Rev. Lett.. **88**, 037001 (2002).
[12] T. Osada *et al.*, Physica (Amsterdam) **18E**, 200 (2003).
[13] A. G. Lebed *et al.*, Phys. Rev. Lett. **93**, 157006 (2004).
[14] D. G. Clarke and S. P. Strong, Adv. Phys. **46**, 545 (1997).
[15] D. B. Gutman and D. L. Maslov, arXiv:cond-mat 0704.0613.
[16] J. Singleton and C. H. Mielke, Contemp. Phys. **43**, 63 (2002).
[17] G. C. Milward *et al.*, Nature (London) **433**, 607 (2005).
[18] P. A. Goddard *et al.*, Phys. Rev. B **69**, 174509 (2004).
[19] J. Singleton *et al.*, arXiv:cond-mat 0606492.
[20] κ-(BEDT-TTF)$_2$Cu(NCS)$_2$'s monoclinic structure means that the interlayer transfer integral is along the a axis, i.e. *not* normal to the conducting planes [18]. Hence, it is labeled $t_{\mathbf{a}}$ rather than $t_\perp$. The monoclinic angle $\beta = 110.3°$ so that the effective $t_\perp \approx 0.94t_{\mathbf{a}}$.
[21] B. J. Powell and R. H. McKenzie, Phys. Rev. B **69**, 024519 (2004).
[22] J. G. Analytis *et al.*, Phys. Rev. Lett. **96**, 177002 (2006).
[23] J. Singleton *et al.*, J. Phys. Condens. Matter **15**, L203 (2003).
[24] B. L. Brandt *et al.* Rev. Sci. Instrum. **70**, 104 (1999).
[25] K. Yamaji, J. Phys. Soc. Jpn. **58**, 1520 (1989).
[26] G. M. Danner *et al.*, Phys. Rev. Lett. **72**, 3714 (1994).
[27] In fact the data show that some vestiges of a 3D FS persist up to at least 50 K [28].
[28] P. A. Goddard *et al.* (to be published).
[29] N. Harrison *et al.*, J. Phys. Condens. Matter **8**, 5415 (1996).
[30] A. Bangura *et al.*, arXiv:cond-mat 0702570.
[31] A. Ardavan *et al.*, Phys. Rev. Lett. **81**, 713 (1998).
[32] K. Kuroki *et al.*, Phys. Rev. B **65**, 100516(R) (2002).
[33] J. Singleton, *Encyclopedia of Condensed Matter Physics*, edited by P. Wyder *et al.* (Elsevier, Oxford, 2005), p. 343.
[34] *Solid State Physics*, edited by N. W. Ashcroft and N. D. Mermin (Holt-Saunders, New York, 1976), p. 347.
[35] *Organic Superconductors* edited by T. Ishiguo, K. Yamaji, and G. Saito (Springer-Verlag, Berlin, 1998).
[36] J. Merino and Ross H. McKenzie, Phys. Rev. B **61**, 7996 (2000).